Development of Hybrid Boundary Integral-Generalized (Partition of Unity) Finite Element Solvers for the Scalar Helmholtz Equation

C. Lu and B. Shanker

2120 Engr. Bldg., Dept. Elec. & Comp. Engr.,

Michigan State University, East Lansing, MI 48824

Abstract

Finite element based techniques have been one of the most popular methods used to model electromagnetic field behavior. Typically, the methods invoked involve representing the function of interest in terms of basis functions whose support is defined over a simplicial mesh. Since its introduction, the technique has seen steady improvement. The method now boasts of adaptive *h*-*p* refinement. Recently, however, Babuska and his colleagues introduced the notion of "meshless finite elements" or the so-called Generalized Finite Element method (GFEM). This method does not rely on an underlying tesselation and admits a larger class of basis functions. Application of this technique to analyze practical problems has largely been restricted to systems that require the solution to the Poisson equation. Investigation of the applicability of this technique to wave scattering problems has been limited. The principal difficulty in analyzing scattering and radiation problems using this technique lies in developing appropriate boundary conditions to truncate the computational domain. Our method of choice is to impose exact boundary conditions using boundary integrals–this is largely governed by the fact that these may be conformal to the surface, and can be readily accelerated using existing fast solvers. We will thoroughly explore the applicability of this technique to two-dimensional electromagnetic systems. In doing so, we will explore the methods necessary to impose various boundary conditions. This analysis will give us the background necessary to develop the framework for hybridizing boundary integral techniques with GFEM, thus imposing an exact radiation boundary condition. The results obtained using this hybrid code will be first validated against analytical data for a range of scenarios. To further validate the proposed approach for more complex scatterers, we integrate GFEM with perfectly matched layers, and compare results obtained for a complex scatterer. Several results that demonstrate the accuracy of the proposed method will also be presented.

Keywords

Generalized Finite Elements, Meshless, hp-adaptive, Boundary Integral

I. Introduction

The state of art of FEM tools for electromagnetic analysis has grown by leaps and bounds over the past few decades [1]. Classical methods require an underlying tesselation on which basis functions are defined. These basis functions are based on a span of polynomials, have finite support, and obey conditions at inter-element boundaries. For instance, Whitney elements that are typically used in computational electromagnetics

satisfy either tangential or normal continuity across inter-element boundaries. A genre of higher order basis functions have also been presented and have been continually refined [2, 3]. Likewise, basis functions that can be used in a h, p-convergence setting have been presented and applied to several engineering problems. Indeed, in a series of excellent papers, it has been shown that it is possible to have true h, p–convergence [4, 5].

Classical FEM schemes require a simplicial structure that satisfies certain aspect ratios to define the span of polynomials. In many situations, creating such a mesh can be laborious and time consuming. For instance, developing h, p-convergence meshes or analyzing time varying phenomena that requires re-meshing at every time instant can be laborious. Another handicap of classical FEM is that the ansatz space used to approximate the local behavior is a span of polynomials. If analytic local behavior is known, then it might be possible to use functions *other than polynomials* to approximate local behavior. The development of "meshless FEM" was motivated by the need to address these possible improvements. Intuitively, these methods work as follows: the domain being considered is partitioned into a union of patches or a "partition of unity," and on these patches, the local approximation is constructed using a span of functions [6]. Thus, the representation of the function is achieved via two functions; one that is defined on the partitions of unity and the other on each of the patches. The basis functions describing the unknowns inherits the higher order nature of approximation from the local basis functions and the smoothness of the functions defined on the partition of unity. As with classical FEM, using a span of different local approximations in different regions is also possible. Thus, the meshless methods retain several features of classical FEM and provide additional flexibility in terms of functions that are used and obfuscating the need for a simplical partition of the domain.

Several flavors of meshless methods exist; the principal difference between these lie in the manner in which the local approximations and functions on patches are specified. However, it has been shown that most of the these methods fit into the framework of the Partition of Unity FEM (PUFEM) or Generalized FEM (GFEM) introduced by Babuska and his colleagues [7, 8]. In what follows, we will use the term GFEM to describe methods to be developed herein. The mathematical foundations of this algorithm have been laid out in great detail [7–9], and it has been shown that h-, p- and hp-adaptivity is easily achieved. Likewise, the efficacy of using a space of harmonic functions as local approximants have been demonstrated [9].

The application of this technique to solving problems in electromagnetics has not been extensive. Principally (this is not a complete list), research has been conducted by [10–21]. To a large extent, our work in this area revolved around developing meshless methods for solving the diffusion equation in both the frequency and time domain as applied to non-destructive evaluation [11–13]. The basis functions used in this analysis relied on the element free Galerkin method (EFG) [22]. The method, particularly its scalar implementation, has been gaining a foothold in the research landscape insofar as application to magnetic field analysis. Recently, we have explored the viability of suitably modifying the EFG method to enable the analysis of

vector fields [15] and have developed meshless-PMLs to enable the analysis of open region problems [23] within the context of the EFG method. However, while the EFG method can be thought of as a subset of GFEM, it does not lend itself readily to *hp*–adaptivity, whereas this is inherent in other GFEM methods. Having a proper understanding of the sources of error and the means though which one may control them is important. We have found that in most of the implementation, reason that the convergence is not of the same order of the underlying scheme is largely due to the improper imposition of boundary conditions.

Proper imposition of boundary conditions within a meshless scheme is challenging. Unlike classical FEM, the space of approximating functions are not *interpolatory*. This poses severe challenges in imposing Dirichlet boundary conditions. More specifically, one cannot use the Lagrange multiplier technique as the approximation spaces have to obey the inf-sup condition, and it is not always possible to construct such spaces for meshless methods. This deficiency is directly linked to the difficulty in truncating the computational domain using boundary integrals. This is due to two facts; (i) to solve the hybrid problem, one typically defines an auxiliary set of basis functions and unknowns to represent the tangential components of the fields [1]. It implies from the above discussion [24] that these basis functions, together with those used in the interior, should satisfy the inf-sup (Babuska-Brezzi) condition, and (ii) there are practical situations wherein one uses a first kind Fredholm integral equation as the boundary is not closed. In these cases, the BI enforces a Dirichlet type condition. Thus, the principal contribution of this paper is four fold:

1. We present a scheme for implementing GFEM for the Helmholtz equation.
2. We develop an adaptation of Nitsche's method for implementing the Dirichlet boundary condition.
3. We develop the hybrid GFEM-BI technique for domain truncation for both open and closed domains.
4. We develop the methodology wherein local boundary conditions can be integrated with GFEM–more specifically, the perfectly matched layer (PML). The development of this technique is a by-product of the need to have an additional modality of validating the results obtained by the GFEM-BI scheme.

Our ultimate aim is to develop a three-dimension vector solver for analyzing electromagnetics. The rationale for embarking upon this specific problem is as follows: (a) This approach presented in this paper (basis functions/means to impose boundary conditions, etc) can readily used for solution of quasi-static electromagnetic phenomena and scalar wave equations; (b) It permits us to work out several mathematical and numerical hurdles–the principal being the application of Dirichlet boundary condition and the accurate evaluation of integrals; (c) it is equally important to understand the manner in which boundary integral based techniques can be hybridized with this scheme. The advantage of hybridizing GFEM with BI is readily apparent; it imposes an exact boundary condition for open domain problems, and the computational cost can be amortized using recent advances in the integral equation technology namely the fast multipole method or a host of FFT-based schemes. This work has provided the mathematical basis for our subsequent work on three-dimensional vector solvers for electromagnetics problems. Our preliminary work in this area was presented recently [**?**], and a paper is being prepared for submission.

This paper proceeds along the following lines; in the next section, we formulate the problem in detail. Here we introduce the concepts of GFEM, discretization of the domain, basis functions, methods for integration, and methods for implementing various boundary condition. The last includes different types of boundary integral techniques and a local absorbing boundary condition. Next, we demonstrate the accuracy and convergence of the GFEM and GFEM-BI via a series of analytical comparisons. We shall also demonstrate the accuracy of this scheme by comparing the results obtained against those obtained by truncating the domain using a PML as an absorbing boundary condition. Finally, the paper will conclude with directions on our future research.

II. Formulation

Consider a multiply connected domain Ω whose interior boundaries are denoted by $\partial\Omega := \Gamma = \bigcup_i \Gamma_i$. It is assumed that this domain is embedded in a domain Ω_e and its exterior boundary Γ_e is defined as $\Gamma_e := \Omega_e \cap \bar{\Omega}$. Interior to the domain Ω, the function $u(x)$ satisfies

$$\begin{aligned} &\left(\nabla \cdot [\alpha(x)\nabla] + \omega^2\gamma(x)\right) u(x) = f(x) \\ &\mathcal{B}_i \{u(x)\} = g_i(x) \quad \text{for } x \in \Gamma_i \\ &\mathcal{B}_e \{u(x)\} = g_e(x) \quad \text{for } x \in \Gamma_e \end{aligned} \tag{1}$$

In the above equations it is assumed that $x \in \mathbb{R}^d$, $\mathcal{B}_e$ and $\mathcal{B}_i$ are differential operators, and $g_i(x)$ is the function that is imposed on Γ_i. Here, $d = 2, 3$, $\alpha(x)$ and $\gamma(x)$ are material parameters. The function of interest $u(x)$ is used to denote the $\hat{z}$ component of either the electric or magnetic field. The rationale of defining Γ_e explicitly is to impose appropriate boundary conditions that enable the analysis of scattering problems. The parameters $\alpha(x)$ and $\beta(x)$ can stand for either the permittivity or permeability, depending on the variable that $u(x)$ represents. Solution to this problem using the standard finite element method requires an underlying tesselation on which basis functions are defined. These basis functions are based on a span of polynomials, have finite support, and obey conditions at inter-element boundaries. For instance, Whitney elements that are typically used in computational electromagnetics satisfy either tangential or normal continuity across inter-element boundaries. Higher order basis functions based on these elements have also been presented and have been continually refined [2, 3]. Likewise, basis functions that can be used in a h, p-convergence setting have been presented and applied to several engineering problems. Indeed, in a series of excellent papers, it has been shown that it is possible to have true hp–adaptivity [4, 5]. On the other hand, meshless methods attach a patch or volumina to each point whose union forms an open covering of the domain. The local shape functions are constructed within each domain. Several different flavors of these methods exists [8]. In this paper we will base our development on the generalized finite element method (GFEM) [8].

A. Generalized Finite Element Method

A.1 Basis functions

The presentation of the fundamentals of basis functions is a repetition of those in [9, 25]. Inclusion of this description is purely for the sake of completeness. GFEM is based on a set of N nodes located at x_i in the vicinity of the domain Ω such that $\left\{x_i \in \mathbb{R}^d : x_i \in \Omega, i = 1, \cdots, N\right\}$. Associated with each of these nodes is a patch or volumina denoted by Ω_i of size h_i such that $\Omega \subset C_\Omega := \bigcup_i \Omega_i$ and $\Omega_i = \left\{x \in \mathbb{R}^d : ||x - x_i|| \leq h_i\right\} \subset \mathbb{R}^d$. Specifically, a patch Ω_i is defined as $\Omega_i = \bigotimes_{k=1}^{d} \Omega_i^{(k)}$, $\Omega_i^{(k)} = \{x^{(k)} \in \mathbb{R}, \mid x_i^{(k)} - x^{(k)} \mid \leq h_i^{(k)}\}$. Figure 1 describes such a construction. Typically, there are no restrictions on the shape of the domain. To a large extent, these are chosen depending on the underlying basis functions. Associated with each patch are basis functions that will be used for Galerkin testing and source. The basis function is a product of two functions, $\psi_i(x)$ and $v_i(x)$: functions $\psi_i(x)$ form a partition of unity subordinate to the cover Ω_i, and a space of functions $v_i(x) = span\left\{v_i^m(x)\right\}$ that are local to the domain Ω_i. The global approximation of the variable is then a space of functions denoted by $V_i(x) = \psi_i(x)v_i(x)$. The basic theory of the GFEM method using this space of functions was originally developed by Babuska and Melenek [9] and is summarized below. Note that the definitions listed below are key to some of the proposed tasks.

Definition : Let $\Omega \in \mathbb{R}^d$ be an open set, and let Ω_i be an open cover of Ω satisfying a point-wise overlap condition

$$\exists M \in N \ \forall x \in \Omega \ \text{card}\left\{i | x \in \Omega_i\right\} \leq M$$

Definition : Let $\{\psi_i\}$ be a Lipchitz partition of unity subordinate to the cover $\{\Omega_i\}$ satisfying the following conditions: (i) $\text{supp}(\psi_i) \subset \Omega_i$ for all i; (ii) $\sum_i \psi_i \equiv 1$ *on* Ω; (iii) $||\psi_i||_{L^\infty(\mathbb{R}^d)} \leq C_\infty$; and (iv) $||\nabla\psi_i||_{L^\infty(\mathbb{R}^d)} \leq \frac{C_\nabla}{\text{diam}(w_i)}$. Here C_∞ and C_∇ are two constants. Then $\{\psi_i\}$ is called an (M, C_∞, C_∇) partition of unity subordinate to $\{w_i\}$. The partition of unity is said to be of degree k if $\psi_i \in \mathcal{C}^k(\mathbb{R}^d)$. The covering sets w_i are called patches.

Assume that the PUM space of functions $V(x) = span\left\{\psi_i v_i\right\}$ is given. Let the function $u_{ap} := \sum_i \psi_i v_i \in V \subset H^1(\Omega)$ be an approximation to $u(x)$. The upper bounds on the error in the function and its gradient have been derived in [9].

The choice of the functions $\psi_i(x)$ and $v_i(x)$ can vary from patch to patch, and is usually dictated by the geometry of the problem. More specifically, the functions $v_i(x)$ can theoretically be modified to include logarithmic singularities. However, the first step of implementing this method is the construction of the patches Ω_i of size h_i that form the open cover for the domain. In general we allow h_i^j, for $j = 1, \cdots, d$ to be different in each dimension. In this paper, we have restricted ourselves to rectangular domains. As the patches Ω_i are to be used in a Galerkin scheme, it is necessary for $\bigcup_i \Omega_i \supset \Omega$. In other words, for any $x \in \Omega$ there exists at least one patch Ω_i that contains x. To develop the cover we use a set of points and psuedo-points as is done in [25]. This will ensure that for $x \in \Omega$ there exists at least one patch such that

$x \in \Omega_i$. Next, the partition of unity functions ψ_i are defined in each Ω_i. By definition, $\sum_i \psi_i(x) = 1 \; \forall \; x \in \Omega_i$. To construct these functions, we use a localized version of Shepard's method [26] that relies on defining a function $\mathcal{W}_i(x)$ with respect to each characteristic point $x_i \in \Omega_i$ such that $\mathcal{W}_i(x) = 0 \; \forall x \in \partial\Omega_i$. In other words, these functions are different from zero only for $x \in \Omega_i$. Several choices for these functions exist; the most common are B-splines of different orders, Gaussian, regularized Lagrangians, etc. The choice of the functions W_i depends on shape of the patch. In this paper, we restrict ourselves to rectangular domains, and therefore, to B-splines of different orders. Then in d-dimensions we construct a function $W_i(x)$ using a tensor product of 1-D functions; i.e., $W_i(x) = \prod_{l=1}^{d} \mathcal{W}\left(\frac{x - x_i^l + h_i^l}{2h_i^l}\right)$. Next, the functions $\psi_i(x)$ are defined by $\psi_i(x) = \frac{W_i(x)}{\sum_{\Omega_k \in C_i} W_k(x)}$, wherein $C_i := \{\Omega_i \in C_\Omega | \Omega_i \bigcap \Omega_j \neq 0\}$.

The partition of unity functions are consistent to first order and higher order approximations are obtained by defining higher order local functions, $v_i(x)$. As mentioned in [9], local approximating functions can be chosen such that they better capture the local behavior of the current. However, we have restricted our choices to either Legendre or Tchebychev polynomials of order P. Thus, in any domain Ω_i the functions $v_i(x) = span\left\{\prod_{l=1}^{d} f_{p(l)}\left(\frac{x^{(l)} - x_i^{(l)}}{h_i^{(l)}}\right)\right\}$ where $p(l) = 0, \cdots, P$.

It is well known that the bilinear form of the differential equation (1) on $H^1(\Omega)$ is

$$\mathcal{A}(u, w) = (f, w) \; \forall \; (u \text{ and } w) \in H^1(\Omega) \tag{2a}$$

$$\mathcal{A}(u, w) = -(\alpha \nabla u, \nabla w) + \omega^2 (\gamma u, w) \tag{2b}$$

where $(\cdot, \cdot)$ denotes the standard inner product in $L^2(\Omega)$. It is apparent that we have not yet incorporated the boundary conditions; the means by which various boundary conditions are incorporated into the variational form will be dealt with exhaustively in Section II-A.3. Using the definitions of basis functions elaborated upon thusfar, $u(x)$ can be now approximated as $u(x) = \sum_i^N I_i V_i$, where N is the total degrees of freedom. Using Galerkin method, the discrete version of this bilinear form can be written as

$$\mathcal{A}\left(u_{i,n}, w_{j,m}\right) = \mathcal{A}\left(\psi_i v_i^n, \psi_j v_j^m\right) \tag{2c}$$

$$\left(f, w_{j,m}\right) = \left(f, \psi_j v_j^m\right) \tag{2d}$$

Note, that the above equations indicate that the interaction between any two domains form block matrices. However, what is crucial in the process is the evaluation of the inner products; this will be dealt with next.

A.2 Evaluation of inner products

The basis functions $V_i(x)$ that were introduced earlier are piecewise rational functions. This is immediately apparent when one examines the construction of $\psi_i(x)$; a different number of functions $W_i(x)$ may contribute to $\psi_i(x)$ at different location. This implies that the quadrature rules must be such that they respect these discontinuities. To overcome these deficiencies, we have followed a method similar to the one proposed by Schweitzer [27]. Here the domain of integration is subdivided into smaller domains where the integrand can

be represented as a product two rational functions. Note that the integrands comprise of products of both $\psi_i(x)v_i^m(x)$ and their derivatives. To illustrate the decomposition of the domain, consider two patches Ω_i and Ω_j that overlap; the domain of overlap is denoted by $C_{ij} := \Omega_i \cap \Omega_j$. Further assume that in each domain, the weight functions $W_i(x)$ and $W_j(x)$ are polynomials of degree l. Then in Ω_i, the function $W_i(x)$ is piecewise rational in $(l+1)^d$–domains. As the function $\psi_i(x)$ is a combination of both $W_i(x)$ and $W_j(x)$ for $x \in \Omega_i$, we can partition the intersection C_{ij} into $C_{ij} = \bigcup_n D_{ij}^n$ disjoint subcells as in Fig. (2), and $\psi_i(x)$ is piecewise rational in each subcell. The process becomes more involved when more than two patches overlap. Such a scenario is illustrated in Fig. (3). Assume $E_{ijk} := \Omega_j \cap \Omega_j \cap \Omega_k$ denotes the domain of intersection of these three domains. It follows that $\bigcup_m F_{ijk}^m \subseteq \bigcup_n D_{ij}^n$ denotes the union of domains wherein the function $\psi_i(x)$ is piecewise continuous. Recursive identification of domains where the function $\psi_i(x)$ is piecewise rational ensures the appropriate construction of quadrature rules.

The above procedure works well for intersection between two domains $C_{ij} := \Omega_i \cap \Omega_j \subset \Omega$. However, if Γ dissects C_{ij}, then it can no longer be considered a union of rectangular domains; see Fig. (4). As before, assume that $C_{ij} = \bigcup_n D_{ij}^n$, and in each D_{ij}^n the functions ψ_i and ψ_j are rational functions. The cells D_{ij}^n are be partitioned into two sets; those that are fully contained within Ω and those that intersect Γ. For the former, we shall use the standard quadrature rules; the latter can be be evaluated through adaptive quadrature. In this paper, we have restricted ourselves to boundaries that are circular. The geometric choice permits the division into rectangular domains and curvilinear triangles as shown in Fig. (4). As before, we use standard quadrature rules in the rectangles, and coordinate transformation and higher order integration in the triangles [1]. Thus, the prescribed procedure enables higher order evaluation of all the inner products in the variational form.

A.3 Imposing boundary conditions

It is evident from the above exposition, that (i) the basis functions V_i are NOT interpolatory; (ii) $\Omega \subset \bigcup_n \text{supp}\,\{V_n\}$. These two facts make imposition of boundary conditions more difficult than those for classical h, p convergence FEM methods. In this section, we will discuss the imposition of both the Nuemann and Dirichlet boundary conditions, as well as the truncation of the domain using boundary integrals.

A.3.a Neumann Boundary Condition:. First, consider the differential equation in (1) with $\mathcal{B}_i\{u(x)\} = \alpha u_n = \alpha \hat{n} \cdot \nabla u(x) = g_n(x)\ \forall x \in \Gamma$. Here, $\hat{n}$ denotes the outward pointing normal from the domain Ω. This boundary condition implies that the bilinear form is to be modified as

$$\mathcal{A}(u, w) = (f, w) - \int_\Gamma dx g_n(x) w(x) \tag{3}$$

From the above, it is apparent that it is sufficient for the trial and basis functions to be in $H^1(\Omega)$. There are no additional constraints, and the basis do not have to satisfy the boundary conditions. Hence, incorporation of Neumann boundary condition is no different than that in classical FEM.

A.3.b Dirichlet Boundary Condition:. Next, assume that $\mathcal{B}_i\{u(x)\} = u(x) = g(x)\ \forall x \in \Gamma$, i.e., Dirichlet boundary condition explicitly imposes the values of $u(x)$ on the boundary of the domain. Alternatively, the problem may be cast as follows: "find $u(x) \in H^1(\Omega)$ such that $u(x) = g(x)\ \forall\ x \in \Gamma$" and the bilinear form for $w \in H^1(\Omega)$

$$\mathcal{A}(u, w) = -\int_\Gamma dx\alpha(x)w(x)\hat{n} \cdot \nabla u(x) + (f, w) \tag{4}$$

This statement is not very different from that posed for standard FEM albeit with a couple of differences: in classical FEM (1) $w \in H_0^1(\Omega)$ which implies that the integral over the boundary vanishes; (ii) the basis functions are interpolatory. Hence, imposing the boundary conditions is tantamount to modifying the linear system. In GFEM, both the trial and test function do not satisfy either of these properties. Thus, imposing Dirichlet boundary conditions is not as straightforward. This has been a topic of considerable discussion [28]. Methods attempted have been (i) to hybridize meshless methods with classical FEM; (ii) use a penalty function method; (iii) use a Lagrange multiplier technique, and (iv) use Nitsche's method. Of the four methods, we have chosen to use Nitsche's method to impose the boundary condition. While we shall discuss this method detail, we shall also dwell briefly on the Lagrange multiplier technique as it will shed light on the constraints on imposing a global boundary condition.

Solving the problem using Lagrange multipliers involves finding a solution $(u, \lambda) \in H^(\Omega) \times H^{-1/2}(\Gamma)$. The formulation can than be stated as follows: given $u(x) \in H^1(\Omega)$ and $\lambda \in H^{-1/2}(\Gamma)$ find the solution to

$$\mathcal{A}_h(u, \lambda; w, \mu) = \mathcal{F}_h\ \forall\ (w \text{ and } \mu) \in H^1(\Omega) \times H^{-1/2}(\Gamma) \tag{5a}$$

$$\mathcal{A}_h = -(\alpha\nabla u, \nabla w) + \omega^2(\gamma u, w) + \langle\lambda, w\rangle + \langle u, \mu\rangle \tag{5b}$$

$$\mathcal{F}_h = (f, w) + \langle g, \mu\rangle \tag{5c}$$

Solution to the discrete version of this equation in the GFEM setting is not trivial. It is well-known that for this problem to converge, it is necessary for both the interior and multiplier spaces to fulfill the Babuska-Brezzi condition. However, it is difficult to design a multiplier space that satisfies this condition [29–31] especially for the space of basis functions being considered here. Moreover, Lagrange multiplier based techniques lead to indefinite systems. An alternative to this could be a stabilized-Lagrange multiplier technique [32]. However, in what follows, we use the Nitsche's technique for imposing the Dirichlet boundary condition. This method is related to the stabilized Largrange multiplier technique with two advantages: (i) it is relatively straightforward to implement in a numerical scheme, and (ii) one does not need to define an additional space of functions in $H^{-1/2}(\Gamma)$. The method proceeds as follows: find an approximate solution

such that $u(x) \in V_N \subset H^1(\Omega)$ such that

$$\mathcal{A}_h(u,w) = \mathcal{F}_h \ \forall w \in V_N \tag{6a}$$

$$\mathcal{A}_h(u,w) = -\left(\alpha\nabla u, \nabla w\right) + \omega^2\left(\gamma u, w\right) + \int_\Gamma dx\ \alpha u\hat{n}\cdot\nabla w + \int_\Gamma dx\ \alpha w\hat{n}\cdot\nabla u - \beta\int_\Gamma dx\ uw \tag{6b}$$

$$\mathcal{F}_h = \left(f, w\right) + \int_\Gamma dx\alpha g\hat{n}\cdot\nabla w - \beta\int_\Gamma dx\ gw \tag{6c}$$

where β is chosen such that it guarantees coercivity. Rigorous estimates exist for β [27]. As is also apparent from the above equations, the resulting system is symmetric.

A.3.c Global Radiation Boundary Condition:. The above exposition has a significant impact on the development of a global boundary condition. In standard FEM-BI expositions [1], one defines equivalent currents on Γ_e, and uses the radiation boundary integral to impose either the electric field or the magnetic field or a combination of both. The equivalent current are of both the electric and magnetic types. As $u(x)$ represents one field (either the electric or magnetic field), either the magnetic or electric currents can be easily obtained. One typically prescribes basis functions for all $x \in \Gamma_e$ to represent currents. However, from our preceding discussion it is apparent that basis functions prescribed on Γ_e have to belong to $H^{-1/2}(\Gamma_e)$, and these functions together with those used in the interior have to satisfy the Babuska-Brezzi condition. While such a space can be easily developed in the case of standard tesselation, it is perhaps not possible for GFEM. Therefore, prescribing additional unknowns on the boundary is ruled out. The method that we use for hybridizing will depend on whether $\Gamma_e = \partial\Omega$ or $\Gamma_e \subset \partial\Omega$. In the former case, the domain of integration encloses a volume, and in the latter, it is open. When the domain is closed, it is sufficient to prescribe conditions such that the solution is unique; i.e., one does not excite the interior resonance modes. While this is a solved problem, it is implementing this condition within the context of GFEM that causes problems. If $\Gamma_e \subset \partial\Omega$, then imposing conditions is considerably more challenging, as imposing the BI is similar to prescribing a Dirichlet boundary condition. This is challenging on two counts; (i) the basis functions V_i are NOT interpolatory; (ii) $\Omega \subset \bigcup_n \text{supp}\left\{V_n\right\}$. Therefore, techniques that were used earlier to overcome this problem [1] need to be modified to impose the boundary condition.

Our formulation proceeds as follows: Assume that just inside the boundary, one can define another surface Γ_s that completely encloses all the inhomogeneities in Ω; see Fig. 5(a). For the purposes of discussion, assume that $u(x)$ refers to the electric field. Then $\forall x \in \Gamma_e$,

$$u(x) = u^{inc}(x) + \mathcal{L}\left\{u(x)\right\} \tag{7a}$$

$$\partial_n u(x) = \partial_n u^{inc}(x) + \mathcal{K}\left\{u(x)\right\} \tag{7b}$$

$$\mathcal{L}\left\{u(x)\right\} \coloneqq -\int_{\Gamma_s} d\Gamma_s\left(\partial_{n'}u(x')g(x,x') - u(x')\partial_{n'}g(x,x')\right) \tag{7c}$$

$$\mathcal{K}\left\{u(x)\right\} \coloneqq \int_{\Gamma_s} d\Gamma_s\left(\partial_{n'}u(x')\partial_n g(x,x') - u(x')g_t(x,x')\right) \tag{7d}$$

where $\partial_{n'}$ and ∂_n are used to denote the normal derivatives with respect to the primed and unprimed coordinates, respectively, $\hat{t} = -\hat{n} \times \hat{z}$, and $u^{inc}(x)$ denotes the incident field. Denoting $r = x - x'$ where $r \in \mathbb{R}^2$, the Green's functions may be written as $g(x, x') = \frac{1}{4j} H_0^2(k|r|)$ and $g_t(x, x') = k^2(\hat{t} \cdot \hat{t'})g(x, x') + \hat{t'} \cdot (\nabla\nabla g(x, x')) \cdot \hat{t}$ where $\hat{t}$ and $\hat{t'}$ are the tangent vectors at x and x', respectively. These equations are essentially derived from surface equivalence theorems (or Huygen's principle). Note, the surfaces Γ_e and Γ_s can be arbitrarily close to each other; however, if they are very close to each other, the integral operators in (7) may be singular/hyper-singular, and one should evaluate these with care. Techniques for doing so are similar to those prescribed in [33]. Next, to incorporate the global boundary condition within the differential equation solver, one needs to specify the differential operator $\mathcal{B}_e\{u(x)\}$ in (1). The simplest is to specify that $\mathcal{B}_e\{u(x)\} = u(x) = u^{inc}(x) + \mathcal{L}\{u(x)\}\ \forall x \in \Gamma_e$. This is, of course, a Dirichlet type boundary condition, and has to be incorporated using Nitsche's method; more specifically by implementing the following

$$\mathcal{A}_h(u, w) = \mathcal{F}_h\ \forall w \in V_N \tag{8a}$$

$$\begin{aligned}\mathcal{A}_h(u, w) = &-(\alpha\nabla u, \nabla w) + \omega^2(\gamma u, w) + \int_\Gamma dx\ \alpha u\hat{n} \cdot \nabla w + \int_\Gamma dx\ \alpha w\hat{n} \cdot \nabla u \\ &- \beta \int_\Gamma dx\ uw - \int_\Gamma dx\alpha\mathcal{L}\{u(x)\}\hat{n} \cdot \nabla w + \beta \int_\Gamma dx\omega\mathcal{L}\{u(x)\}\end{aligned} \tag{8b}$$

$$\mathcal{F}_h = (f, w) + \int_\Gamma dx\alpha u^{inc}\hat{n} \cdot \nabla w - \beta \int_\Gamma dx\ u^{inc}w \tag{8c}$$

Alternatively, one can specify $\mathcal{B}_e\{u(x)\} = \partial_n u(x) = \partial_n u^{inc}(x) + \mathcal{K}\{u(x)\}\ \forall x \in \Gamma_e$. As before, this is the Neumann type boundary condition, and can be incorporated by appropriately modifying the variational formulation. However, it is well known that both global boundary conditions do not yield unique solutions at all frequencies. These frequencies correspond to the null spaces of the appropriate operators [1]. Among the several methods prescribed [1] to overcome this deficiency, one is to combine the two operators; i.e., use a combined field formulation. Thus, the method proceeds as follows: find an approximate solution $u(x) \in H^1(\Omega)$ such that

$$\mathcal{A}_h(u, w) = \mathcal{F}_h\ \forall w \in H^1(\Omega) \tag{9a}$$

$$\mathcal{A}_h(u, w) = -(\alpha\nabla u, \nabla w) + \omega^2(\gamma u, w) - jk \int_{\Gamma_e} dxw(x)u(x) + \int_{\Gamma_e} dx\ w(x)\left[jk\mathcal{L}\{u(x)\} + \mathcal{K}\{u(x)\}\right] \tag{9b}$$

$$\mathcal{F}_h = (f, w) - \int_{\Gamma_e} dxw(x)\left[jku^{inc}(x) + \partial_n u^{inc}(x)\right] \tag{9c}$$

In the above exposition, we have essentially focused on imposing the boundary condition at Γ_e. As in (1), another condition might need to be imposed in the interior boundaries. However, as is apparent, the bilinear form for imposing these conditions may be derived trivially using material presented thusfar. Evaluation of the integrals over the boundary may be carried out using several different methods. In our implementation, we proceed as follows: The domain of integration (either Γ_s or Γ_e can be partitioned into a union of subdomains over with the basis function is piecewise smooth. Then over each such subdomain, we use a

Gauss-Legendre quadrature. While this is not truly optimal and one may construct better quadrature rules, we did obtain convergent results.

A.3.d Local Radiation Boundary Condition:. Our interest in implementing the local boundary condition is purely to develop another measure of validating the results obtained using global boundary condition. As we will show, the results obtained using GFEM-BI converge exponentially to analytical solutions. However, as these solutions are available only for canonical problems, it is of interest to know that the fields obtained using the afore-developed scheme and those obtained using a local boundary condition agree with each other. There is a wealth of local boundary conditions that are available [1, 34]. Here we implement a perfectly matched layer (PML) within GFEM. The literature on PML is extensive, and our goal is to present a rudimentary development that can be used as a validation modality. The approach that we use to implement this relies on the stretched coordinate system first introduced in [35]. Using this technique results in a slight change in $\alpha(x)$ in that it becomes a tensor of rank 2, i.e., $\bar{\alpha}(x) = \alpha_0 \alpha_{ij}(x)$. The quantity $\tilde{\gamma}(x)$ and the non-zero elements of $\bar{\alpha}(x)$ are

$$\begin{aligned} \alpha_{11}(x) = \alpha_0 \frac{s_1(x)}{s_2(x)} \qquad \alpha_{22}(x) = \alpha_0 \frac{s_2(x)}{s_1(x)} \\ \tilde{\gamma}(x) = \gamma_0 s_1(x) s_2(x) \end{aligned} \tag{10}$$

where $x = (x_1, x_2)$, α_0 and γ_0 are appropriate constants when all stretching parameters are one, and

$$s_1(x) = 1 - j\frac{\sigma_{11}(x_1)}{\omega\varepsilon_0} \qquad s_2(x) = 1 - j\frac{\sigma_{22}(x_2)}{\omega\varepsilon_0} \tag{11}$$

In these equations, s_1 and s_2 are stretching coordinates, and $\sigma_{ij}(x)$ denotes the conductivity tensor of the domain. As is apparent, this tensor is chosen to be diagonal. The domain of application of the PML is denoted using $\Omega_{PML} = \Omega_0 - \Omega_i$, where the rectangular domains Ω_0 and Ω_i are defined as $\Omega_0 = x_1^2 \times x_2^2$ and $\Omega_i = x_1^1 \times x_2^1$; see Fig. 5(b). The conductivity profiles are chosen to be zero inside the Γ_i and vary quadratically in the direction of the outward normal to the boundary Γ_i. σ_{11} is nonzero in domain $(-0.5x_1^2, -0.5x_1^1) \times (-0.5x_2^2, 0.5x_2^2)$ and $(0.5x_1^1, 0.5x_1^2) \times (-0.5x_2^2, 0.5x_2^2)$, σ_{22} is nonzero in domain $(-0.5x_1^2, 0.5x_1^2) \times (-0.5x_2^2, -0.5x_1^2)$ and $(-0.5x_1^2, 0.5x_1^2) \times (0.5x_2^1, 0.5x_2^2)$. Finally, the computational domain is truncated by imposing the condition

$$\hat{n} \cdot \nabla u^s + jk\cos(\theta_a) u^s = 0 \tag{12}$$

on Γ_0. Here, θ_a denotes the angle of perfect absorption and is chosen to be $\theta_a = \frac{\pi}{3}$ in our simulation. Note that in this formulation, the unknown is scattered field u^s. With these changes, the bilinear form may now

be written as

$$\mathcal{A}_h(u^s, w) = \mathcal{F}_h \ \forall w \in V_N \tag{13a}$$

$$\mathcal{A}_h(u^s, w) = -\left(\bar{\alpha} \cdot \nabla u^s, \nabla w\right) + \omega^2 \left(\tilde{\gamma} u^s, w\right) - jkcos(\theta_a) \int_\Gamma dx \ u^s w \tag{13b}$$

$$\mathcal{F}_h = \left(f, w\right) - \left(\alpha \nabla^2 u^{inc}, w\right) - \omega^2 \left(\gamma u^{inc}, w\right) \tag{13c}$$

III. Numerical experiments

In what follows, we shall present a series of numerical experiments that will serve to demonstrate the accuracy and convergence of the method presented herein. In all examples presented below, we have chosen $d = 2$ merely for demonstration purposes, and as is evident from the presentation, extension to $d = 3$, is relatively easy albeit at considerable more programming cost. First, we shall demonstrate h, p convergence for problems wherein either the Dirichlet or Neumann boundary conditions are specified. Next, we shall demonstrate similar convergence for our hybrid GFEM-BI scheme and also demonstrate that our scheme is free from corruption due to interior resonance modes. In these examples, global boundary conditions are used to truncate the computational domain, and Dirichlet boundary conditions are imposed in the interior of the domain. Finally, we present a set of results that analyze electrically large problems, and compare these against either analytical results or against GFEM augmented with local boundary truncation schemes. While meshless methods offer a host of advantages, one significant hurdle/unsolved problem is the conditioning of the resultant linear system as the order of the basis function increases. This is an issue when we are trying to demonstrate h, p convergence. In these cases, we resort to an SVD-based solver. However, in the analysis of electrically large objects, wherein we are satisfied with an error in the L_2-norm = 1e-4, we use a non-stationary iterative solver like TFQMR [36] with block preconditioners.

In the next two examples, we demonstrate h, p convergence of this method when imposing either the Neumann or the Dirichlet boundary condition. The domain of analysis of both problems are the same and defined as follows: the domain of interest $\Omega = (0,1)^2$, and the boundary $\Gamma = \bigcup_i^4 \Gamma_i$ where $\{\Gamma_1 : x \in 0 \times (0,1)\}$, $\{\Gamma_2 : x \in (0,1) \times 1\}$, $\{\Gamma_3 : x \in 1 \times (0,1)\}$, and $\{\Gamma_4 : x \in (0,1) \times 0\}$.

In the first example, the Neumann boundary conditions are imposed on all four walls. More specifically, $\mathcal{B}_i \left\{u(x)\right\} = \partial_n u(x)|_{\forall x \in \Gamma_i} = g_i(x)$. Denoting $x = (x_1, x_2)$, $g_i(x) = 0, -2.97\cos(4x_1), 3.0272\sin(3x_2), 3\cos(4x_1)$, for $i = 1, \cdots .4$. The above boundary conditions permit analytical solution of the (1). In this experiment, all nodes are distributed uniformly, and rectangular patches are used. The size of each patch is chosen to be 1.5 times the distance between the nodes. The weight functions $W_i(x)$ is a product rooftops, and the approximation is a tensor product of Legendre polynomials. Two sets of results are shown. In the first, we demonstrate the error between analytical and numerical solutions in Fig. 6 for $h = 0.11\lambda$ and $p = 4$. We also demonstrate h, p convergence in Fig. 7. As is evident from the graphs, the results are excellent.

Next, the Dirichlet boundary condition is imposed on all four walls. More specifically, $\mathcal{B}_i \left\{u(x)\right\} =$

$u(x)|_{\forall x\in\Gamma_i} = g_i(x)$. Denoting $x = (x_1, x_2)$, $g_i(x) = \sin(3x_2), 0.1411\cos(4x_1), -0.6536\sin(3x_2), 0$, for $i = 1, \cdots .4$. All the parameters used in the computation are the same as those used for imposing the Neumann boundary condition. Again, the Fig. 8 plots the relative value of the error in the entire computational domain when using $h = 0.11\lambda$ and $p = 4$. Also, the errors for different values for h and p are shown in Fig. 9. It is evident that Nitsche's method for imposing the boundary conditions shows excellent convergence.

Next, we examine the accuracy of imposing the boundary integral to truncate the domain. To do so we analyze scattering from a perfect electrically conducting (PEC) cylinder and the truncation boundary is placed 0.1λ away from the surface. Given the configuration of the problem, we need to apply the BI (CFIE) (9a) and Dirichlet boundary condition on the truncation boundary Γ_e and the inner boundary, respectively. We compare these results against that obtained analytically to obtain the h, p convergence graphs in Fig. 10(a). As is evident, the scheme presented in this paper demonstrates the anticipated convergence characteristics. The next, we analyze scattering from a PEC cylinder over a range of frequencies. The outer boundary is truncated using the EFIE specified in (8a), and the inner boundary is truncated using a Dirichlet boundary condition. We know that truncating the outer boundary with the EFIE would lead to unique values for all values of ka except those that correspond to interior resonance modes of a cylinder with a PEC wall at the outer boundary. Thus, to satisfy ourselves that this is indeed the case, and to show that the variational form that imposes the EFIE formulation presented in this paper is valid (note: EFIE is imposed using Nitsche's method), we analyze scattering from a cylinder over a range ka varying from 2.0 to 8.0 in steps of 0.05. Additionally, values of ka that are within three digits of the resonance frequencies corresponding to TM^z modes of the cylinder whose radius corresponds to that of Γ_e are chosen. In total, we ran this simulation for a total of 128 frequency points. In all cases, $h = 0.1\lambda$ and $p = 3$. Figure 10(b) compares the error in the field values within the computational domain to analytical data. As is expected, Fig. 10(b) shows the results obtained are accurate except at resonance frequencies. So, the next challenge is to ensure that our results are free of corruption by spurious modes. Again, we analyze scattering from a PEC cylinder over a range of frequencies with combined boundary integral formula. It is apparent from Fig. 10(c) that the error is fairly constant over the entire band of frequencies. It should be noted that in all the cases mentioned thus far, we are quoting the error in the field values at a sufficient dense set of samples inside the computational domain. These error are NOT in the echo width data, as they tend to be significantly smaller.

Next, we demonstrate the applicability of this technique to various scattering problems. In all three examples described, the incident plane wave propagates along the $\hat{x}$ direction and is polarized along $\hat{z}$. First, scattering from a cylinder of radius 2.7λ is analyzed. The source boundary Γ_s and fictitious boundary Γ_e are at 2.85λ and 3.0λ, respectively, and $h = 0.11\lambda$ and $p = 3$. The analytical and numerical data of electric field on fictitious boundary and echo width (EW) are compared in Fig. 11. As is evident from these graphs, the results are excellent. Next, scattering from dielectric-coated PEC cylinder is analyzed. The radius of

the PEC cylinder is 2.82λ, and the thickness of the dielectric coating is 0.06λ. The relative permittivity of dielectric is 2.0. The source boundary Γ_s and fictitious boundary Γ_e are at 2.94λ and 3.0λ, respectively, where λ is the free space wavelength and $h = 0.12\lambda$ and $p = 3$. The analytical and numerical data of the electric field on fictitious boundary and echo width (EW) are compared in Fig. 12. As is evident from these graphs, the results are excellent. Finally, we analyze scattering from a coated cylinder that is considerably larger. The radius of cylinder PEC and dielectric coating are 3.76λ and 3.84λ, respectively. The source boundary Γ_s and fictitious boundary Γ_e are at 3.92λ and 4.0λ, respectively. As before, λ is the free-space wavelength, $\varepsilon_r = 2$, $h = 0.15\lambda$ and $p = 3$. Our discretization in this case is considerably coarser, however, as is evident from Fig. 13 (a,b), both the fields on the fictitious surface and the echo-width agree very well with the analytical data.

In the last example, we compare the results obtained using GFEM-BI with those obtained by analyzing the same object using GFEM-PML. As is well known, the principal advantage of the boundary integral is that realized by a reduced computational domain. This, of course, implies that the cost of application of the BI can be reduced to something that scales almost linearly with the number of unknowns on the boundary. This is indeed possible by augmenting the BI with acceleration techniques, notably by the fast multipole technique [37]. The object that we choose for simulation is a L-shaped dielectric scatterer. The length and width of each arm is 1λ and 0.3λ, respectively, and the arms are oriented along the $\hat{x}$ and $\hat{y}$ directions. The truncation boundary Γ_e for the BI is conformal to the scatterer and is at a distance of 0.25λ away from the scatterer. When employing the PML, the scatterer is embedded in an rectangular domain of size $\Omega_i = 5.4 \times 5.4\lambda^2$, and the thickness of the PML is 0.95λ. In both simulations, $h = 0.08\lambda$ and $p = 3$, and the relative dielectric constant $\varepsilon_r = 2$. The incident field is $\hat{z}$ polarized and propagates along $\hat{k} = -1/\sqrt{2}\,(\hat{x} + \hat{y})$. Figure 14(a,b) show the fields obtained by both methods. As is evident, they are identical to each other. Indeed, the relative error in the field values at a set of points in the domain is 2.3e-3, indicating that both techniques compare very well with each other.

IV. Conclusions

Generalized finite element techniques have not been extended extensively to applications that involve the Helmholz equation; as was noted earlier, aside from a small community, there is a paucity of researchers using this approach to problems in applied electromagnetics. This may largely be attributed to the lack of details on all implementation aspects of this technique as well as difficulties associated with imposing boundary conditions that are commonly encountered in electromagnetics. This paper addresses several of these issues in detail, and demonstrates for a range of "scalar" problems that this method does indeed work well. To make this technique widely applicable, we have developed the first hybrid GFEM-BI technique that enables the truncation of the computational domain, and demonstrated its h, p convergence properties. As was noted, we have specified the manner in which different types of boundary integrals may be incorporated into

the simulations. Validating the proposed technique for scattering from more complex shapes necessitated the development of GFEM-PML techniques. However, to make this technique truly applicable to a wide class of problems in electromagnetics, one needs to develop vector basis functions that satisfy the de-Rham map. Preliminary results of this results have been presented recently [**?**], and a full paper detailing these ideas and results is being prepared.

References

[1] J. M. Jin, *The Finite Element Method in Electromagnetics*. New York: Wiley, 2002.

[2] R. D. Graglia, D. R. Wilton, and A. F. Peterson, "Higher order interpolatory vector bases for computational electromagnetics," *IEEE Transactions on Antennas and Propagation*, vol. 45, pp. 329–342, 1997.

[3] W. Rachowicz and L. Demkowicz, "A three-dimensional hp-adaptive finite element package for electromagnetics." TICAM Report 00-04, 2000.

[4] M. Costabel, M. Dague, and C. Schwab, "Exponential convergence of hp-fem for maxwell's equations with weighted regularization in polygonal domains," *Mathematical Models and Methods in Applied Sciences*, vol. 15, 2005. To Appear: paper available at http://perso.univ-rennes1.fr/monique.dauge/core/index.html.

[5] D. Boffi, M. Costabel, M. Dague, and L. Demkowicz, "Disscrete compactness for the *hp* version of rectangular edge finite elements." ICES Technical Report 04-29, 2004.

[6] S. N. Atluri and S. Shen, *The Meshless Local Petrov Galerkin Method*. Tech. Sci. Press, 2002.

[7] I. Babuska and J. M. Melenek, "The partition of unity method," *International Journal for Numerical Methods in Engineering*, vol. 40, pp. 727–858, 1997.

[8] I. Babuska, U. Banerjee, and U. Osborn, "Meshless and generalized fem: A survey of some major results," in *Meshfree Methods for Partial Differential Equations* (M. Griebel and M. A. Sciweitzer, eds.), Springer Verlag, 2002.

[9] J. M. Melenek and I. Babuska, "The partition of unity finite element method: Basic theory and applications," *Comput. Methods Appl. Mech. Engr.*, vol. 139, pp. 289–314, 1996.

[10] L. Xuan, B. Shanker, and L. Udpa, "A meshless element free galerkin method for nde applications," in *Proceedings of Appliced Computational Electromagnetics Society*, 2002.

[11] L. Xuan, B. Shanker, Z. Zeng, and L. Udpa, "Element-free galerkin method in pulsed eddy currents," *The International Journal of Applied Electromagnetics and Mechanics*, vol. 19, pp. 463–466, 2004.

[12] L. Xuan, Z. Zeng, B. Shanker, and L. Udpa, "Development of a meshless finite element model for nde applications," *IEEE Transactions on Magnetics*, vol. 40, pp. 12–20, 2004.

[13] L. Xuan, Z. Zheng, B. Shanker, and L. Udpa, "Numerical modeling using meshless methods for pulsed eddy current phenomena," *IEEE Transaction on Magnetics*, 2004. To appear.

[14] L. Chuan, B. Shanker, and L. Kempel, "Partition of unity methods in electromagnetics," in *Proceedings of the URSI-EM Theory Symposium*, p. 331, 2004.

[15] Z. Zheng, L. Xuan, B. Shanker, L. Kempel, and L. Udpa, "Development of vector basis function for meshless efg method." Presented at URSI, 2003, 2003.

[16] I. Tsukerman, "A flexible local approximation method for electro- and magnetostatics," *IEEE Transactions on Magnetics*, vol. 40, pp. 941 – 944, 2004.

[17] A. Plaks, I. Tsukerman, and G. F. B. Yellen, "Generalized finite-element method for magnetized nanoparticles," *IEEE Transactions on Magnetics*, vol. 39, pp. 1436 – 1439, 2003.

[18] I. Tsukerman, "Spurious numerical solutions in electromagnetic resonance problems," *IEEE Transaction on Magnetics*, vol. 39, pp. 1405 – 1408, 2003.

[19] I. Tsukerman, "General tangentially continuous vector elements," *IEEE Transactions on Magnetics*, vol. 39, pp. 1215 – 1218, 2003.

[20] L. Proekt, S. Yuferev, and I. T. N. Ida, "Method of overlapping patches for electromagnetic computation near imperfectly conducting cusps and edges," *IEEE Transaction on Magnetics*, vol. 38, pp. 649 – 652, 2002.

[21] L. Proekt and I. Tsukerman, "Method of overlapping patches for electromagnetic computation," *IEEE Transaction on Magnetics*, vol. 38, pp. 741 – 744, 2002.

[22] T. Belytschko, Y. Krongauz, D. Organ, M. Fleming, and P. Krysl, "Meshless methods: An overview and recent developments," *Comp. Meth. Appl. Mech.*, 1996.

[23] Z. Zheng, B. Shanker, and L. Udpa, "Modeling microwave nde using the element free galerkin method–development of perfectly matched layers for domain truncation," in *Proceedings of the Tenth International Workshop on Electromagnetic Non-destructive Evaluation*, 2004.

[24] G. C. Hsiao and R. E. Klienmann, "Mathematical foundations for error estimation in numerical solutions of integral equations in electromagnetics," *IEEE Trans. Antennas Propagat.*, vol. 45, pp. 316–328, 1997.

[25] M. Griebel and M. A. Schweitzer, "Particle-partition of unity methods for pdes," *SIAM J. Sci. Compt*, vol. 22, pp. 853–890, 2002.

[26] D. Shepard, "A two-dimensional interpolation function for irregularly spaced data," in *Proceeding of ACM*, p. 517524, 1968.

[27] M. Griebel and M. A. Schweitzer, *Meshless Methods for Partial Differential Equations*. Springer Verlag, 2002.

[28] S. Fernández-Méndez and A. Huerta, "Imposing essential boundary conditions in mesh-free methods," *Comput. Methods Appl. Mech. Engrg.*, vol. 193, pp. 1257–1275, 2004.

[29] J. Pitkäranta, "Boundary subspaces for the finite element method with lagrange multipliers," *Numer. Math.*, vol. 33, pp. 273–289, 1979.

[30] J. Pitkäranta, "Local stability conditions for the babuska method of lagrange multipliers," *Math. Comput.*, vol. 35, pp. 1113–1129, 1980.

[31] J. Pitkäranta, "The finite element method with lagrange multipliers for domain with corners," *Math. Comput.*, vol. 37, pp. 13–30, 1981.

[32] R. Stenberg, "On some techniques for approximating boundary conditions in the finite element method," *Journal of Computational and Applied Mathematics*, vol. 63, pp. 139–148, 1995.

[33] L. F. Canino, J. J. Ottusch, M. A. Stalzer, J. L. Visher, and S. M. Wandzura, "Numerical solution of the helmholtz equation in 2d and 3d using a high-order nystrm discretization," *J. Comput. Phys.*, vol. 146, pp. 627–663, 1998.

[34] W. C. Chew, *Waves and fields in inhomogeneous media*. New York: IEEE Press, 1995.

[35] W. C. Chew and W. H. Weedon, "A 3d perfectly matched medium from modified maxwell's equations with stretched coordinates," *Microwave Opt. Technol. Lett.*, vol. 7, pp. 599–604, 1994.

[36] Y. Saad, *Iterative Methods for Sparse Linear Systems*. New York: PWS Publishing Company, 1996.

[37] V. Rokhlin, "Rapid solutions of integral equations of scattering theory in two dimensions," *J. Comput. Phys.*, vol. 86, pp. 414–439, 1990.

List of Figures

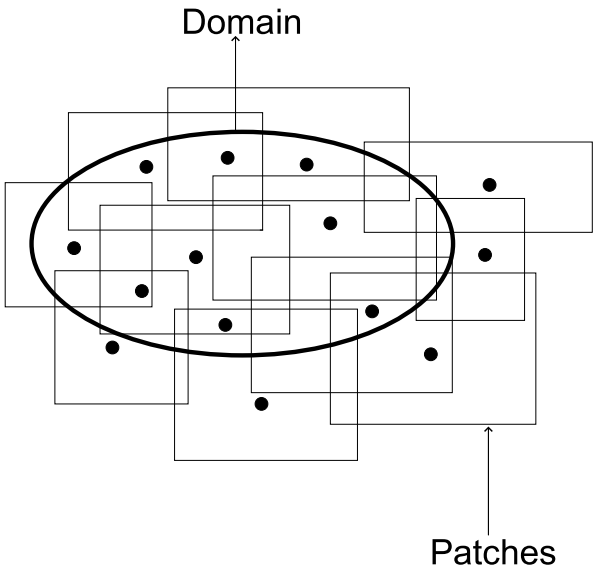

Fig. 1. Construction of the computational domain.

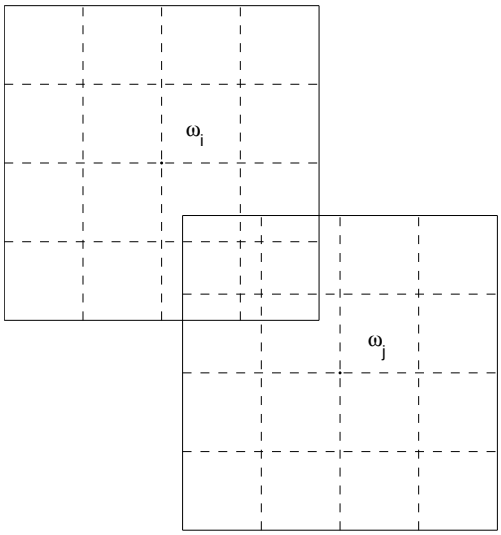

Fig. 2. Subdivision of the domain of integration based on piecewise weight function W_i.

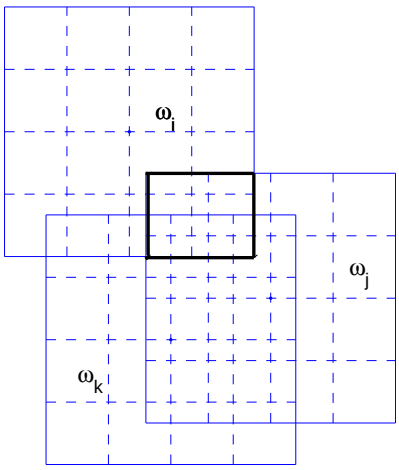

Fig. 3. Subdivision of D_{ij}^n based on the number of patches at different location.

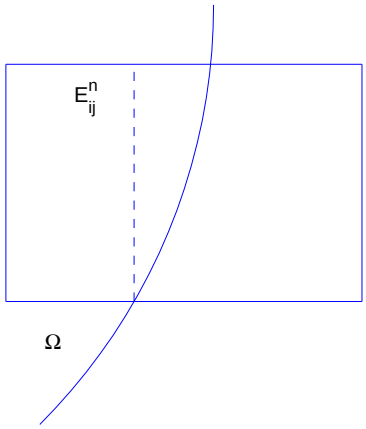

Fig. 4. Integration in the sub-patch E_{ij}^n that overlaps with boundary of computation domain Γ.

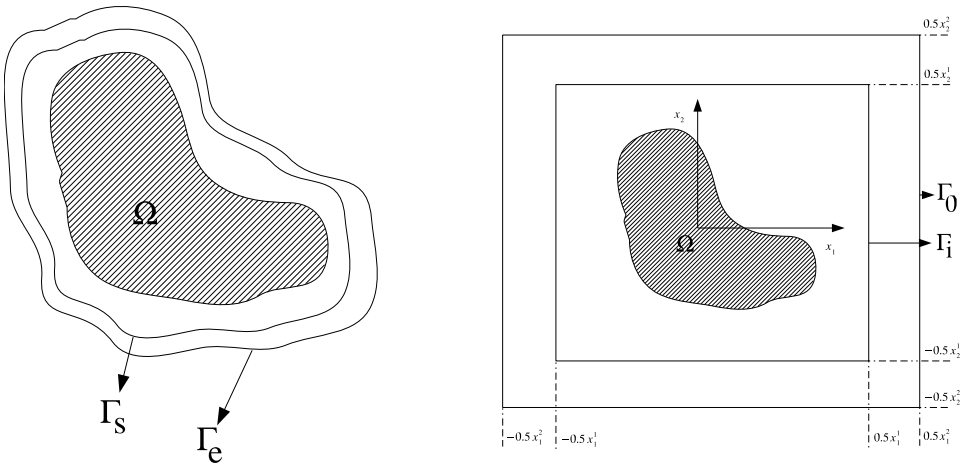

(a) Boundary Integral domain description

(b) PML domain description

Fig. 5. (a) Definition of geometry for imposing the boundary integral; (b) Definition of the geometry for application of the PML.

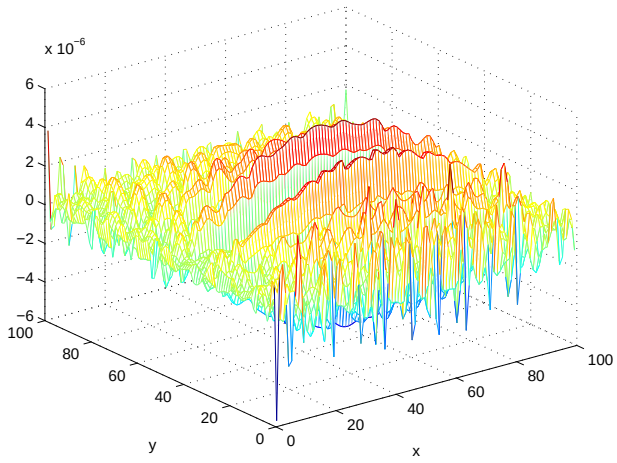

Fig. 6. Error in the L_2 norm of the numerical and analytical solutions of the PDE with the Neumann boundary condition.

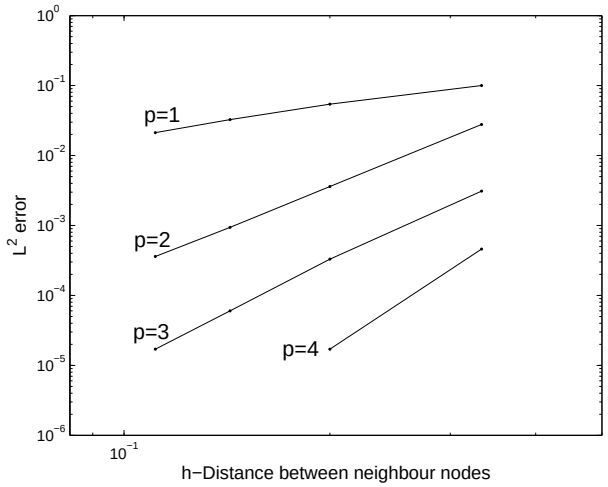

Fig. 7. h, p convergence of the numerical scheme applied to the solution of a PDE with Neumann boundary conditions.

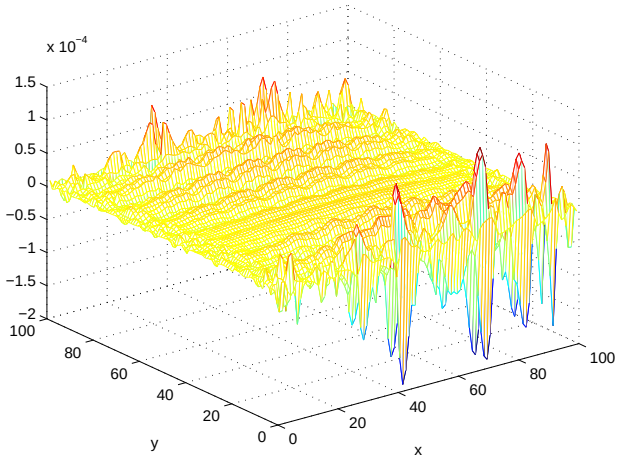

Fig. 8. Error in the L_2 norm of the numerical and analytical solutions of the PDE with the Dirichlet boundary condition.

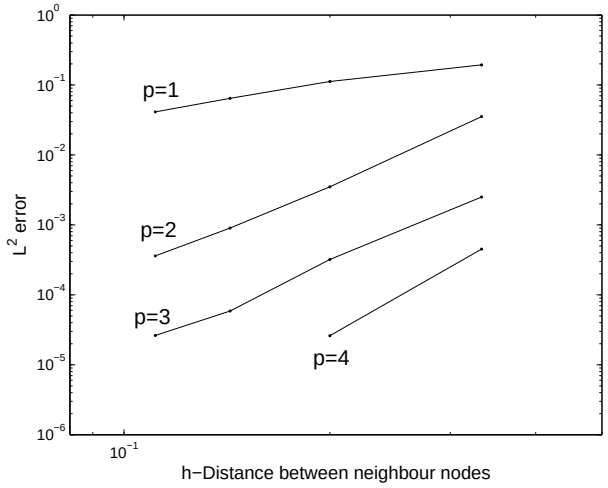

Fig. 9. h, p convergence of the numerical scheme applied to the solution of a PDE with Dirichlet boundary condition.

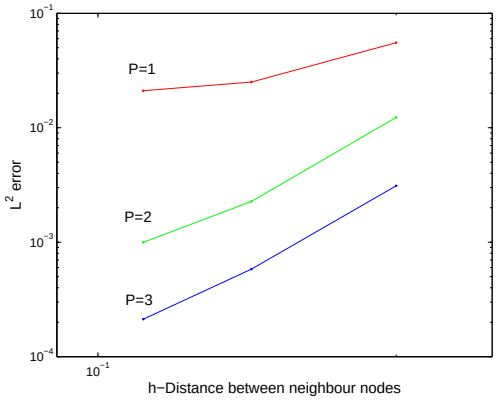

(a) h, p convergence of GFEM-BI (CFIE)

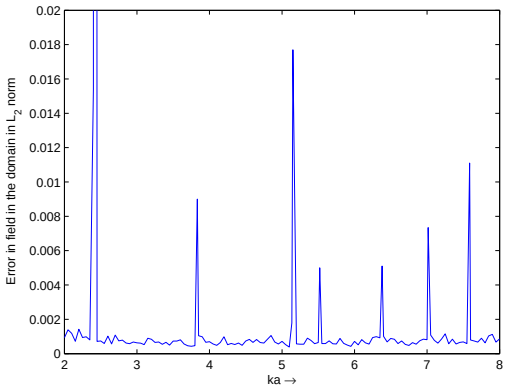

(b) Error in L_2 norm using GFEM-BI (EFIE)

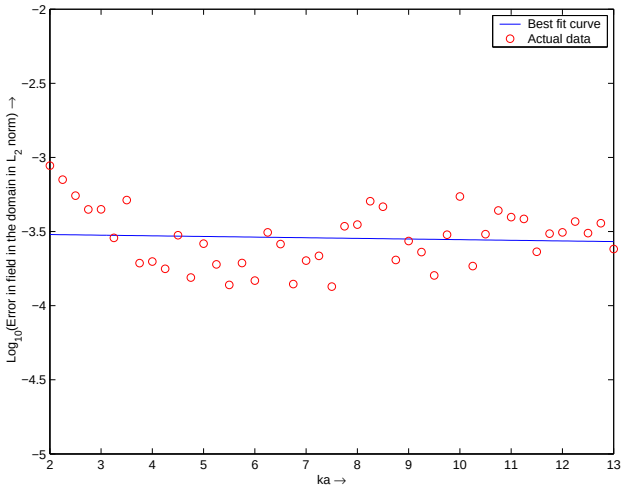

(c) Error in L_2 norm using GFEM-BI (CFIE)

Fig. 10. (a) h, p convergence of the GFEM-BI scheme; (b) Error in E-field over a range of ka with GFEM-BI (EFIE) (c) Error in E-field over a range of ka with GFEM-BI (CFIE).

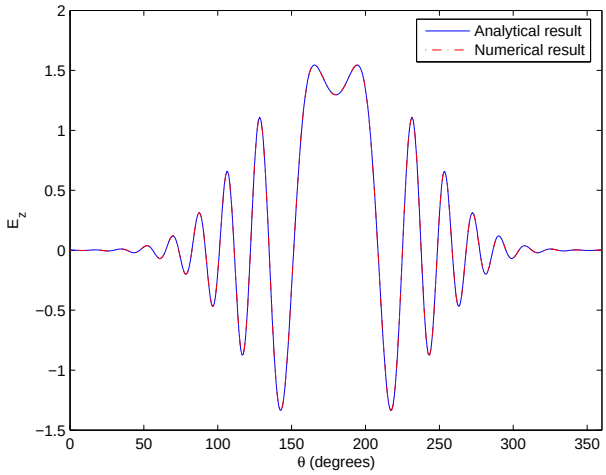

(a) E_z on fictitious boundary Γ_e

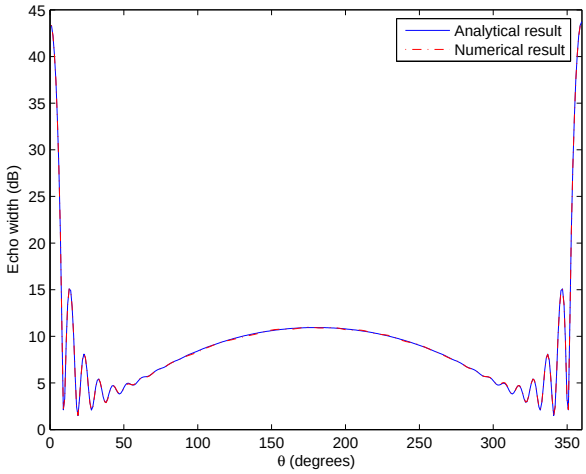

(b) Echo width (EW)

Fig. 11. Comparison between numerical and analytical data obtained for scattering from a perfectly conducting cylinder of radius 2.7 λ: (a) the electric field at Γ_e; (b) Echo-width of the cylinder.

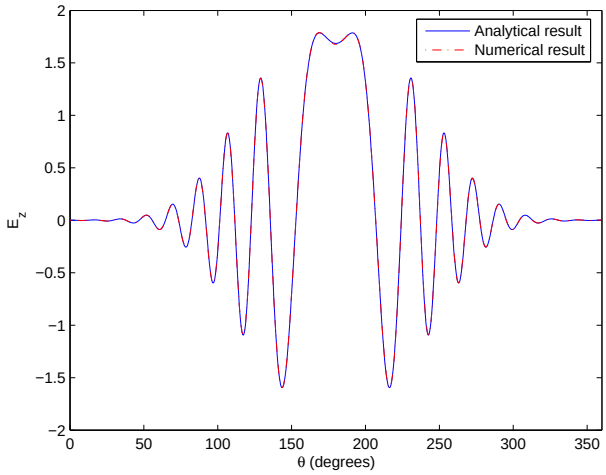

(a) E_z on fictitious boundary Γ_e

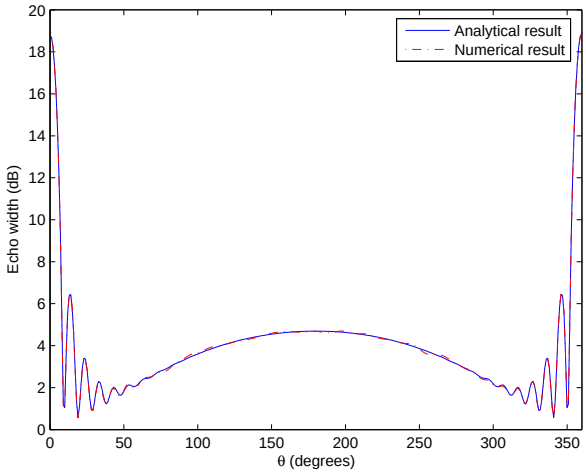

(b) Echo width (EW)

Fig. 12. Comparison between numerical and analytical data obtained for scattering from the coated perfectly conducting cylinder if radius 2.88 λ: (a) the electric field at Γ_e; (b) Echo-width of the cylinder.

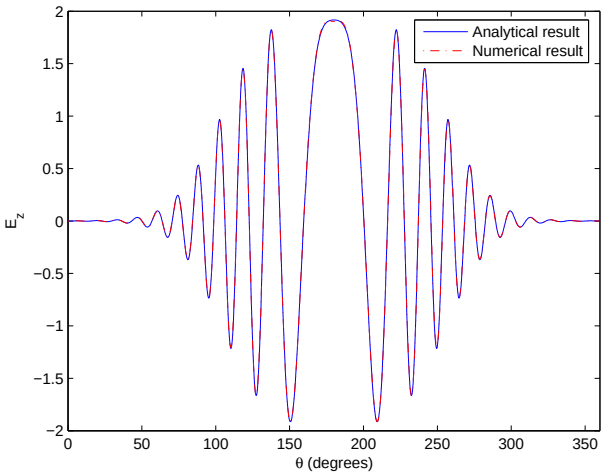

(a) E_z on fictitious boundary Γ_e

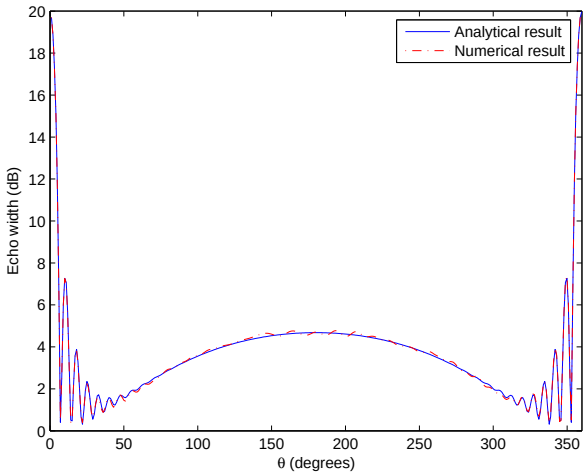

(b) Echo width (EW)

Fig. 13. Comparison between numerical and analytical data obtained for scattering from a coated perfectly conducting cylinder of radius 3.84 λ: (a) the electric field at Γ_e; (b) Echo-width.

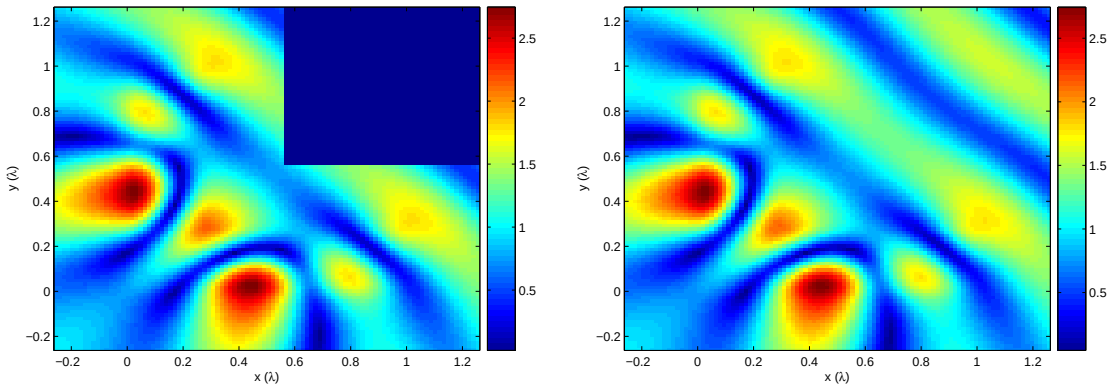

(a) GFEM-BI (b) GFEM-PML

Fig. 14. Comparison of data obtained for scattering from an L-shaped object using GFEM-BI and GFEM-PML.